# On the Phase Behavior of Binary Mixtures of Nanoparticles

Avi Ben-Simon, Hagai Eshet, and Eran Rabani*

School of Chemistry, The Sackler Faculty of Exact Sciences, Tel Aviv University, Tel Aviv 69978, Israel

ABSTRACT The assembly of mixtures of nanoparticles with different properties into a binary nanoparticle superlattice (BNSL) provides a route to fabricate novel classes of materials with properties emerging from the choice of the building blocks. The common theoretical approach based on the hard-spheres model predicts crystallization of only a few metastable binary superstructures (NaCl, AlB$_2$ or the AB$_{13}$). Recently [Shevchenko, E. V.; Talapin, D. V.; O'Brien, S.; Murray, C. B. *Nature* 2006; *439*, 55.)], it has been demonstrated that with the use of a combination of semiconducting, metallic, and magnetic nanoparticles, a variety of novel BNSL structures were formed, where at least 10 were low density structures that have not been previously reported. While some of the structures can be explained by the addition of electrostatic interactions, it is clear that at the nanometer scale one needs to consider other influences, such as van der Waals forces, steric effects, *etc.* Motivated by those experiments, we study, using Monte Carlo simulations, the phase behavior of binary mixtures of nanoparticles interacting *via* a combination of hard-core electrostatics and van der Waals forces. We include a tuning parameter that can be used to balance between electrostatic and dispersion interactions and study the phase behavior as a function of the different charges and size ratios of the nanoparticles. The results indicate that at the nanoscale, both electrostatic and dispersion interactions are necessary to explain the experimental observed BNSL structures.
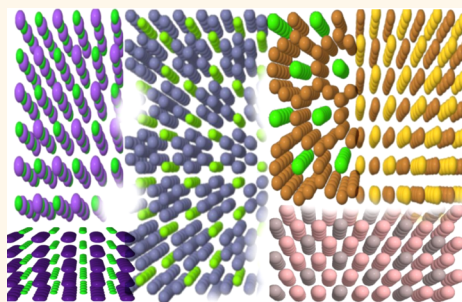
KEYWORDS: self-assembly · Monte Carlo simulations · free energy · binary crystals · dispersion and electrostatic interactions

The growing interest in the self-assembly of binary mixtures of nanoparticles into superlattices is driven both by fundamental and applied aspects. From the practical point of view, such metamaterials may exhibit interesting physical properties, such as negative refractive index or superlenses capable of imaging objects that are much smaller than the wavelength of light.[1−3] From a fundamental perspective, the self-assembly of binary mixtures is still a great mystery. The pioneering work of Shevchenko, Talapin, O'Brien, Murray, and co-workers[4−9] on the structural diversity of binary nanoparticle superlattices along with the intriguing recent discovery of quasicrystalline order in self-assembled binary nanoparticle superlattices,[10] are not well understood.

Of particular importance to the present study is the work of Shevchenko *et al.*,[8] who demonstrated the formation of more than 15 different binary superlattice structures; 10 of them were never reported before.[8] The common wisdom based on the hard spheres (HS) model[11−13] leads to the formation of a variety of superstructures such as the face centered cubic (fcc), the hexagonal closed packing (hcp), rocksalt (NaCl), AlB$_2$ or the AB$_{13}$ (NaZn$_{13}$), all in maximal packing volume fractions.[14] The fcc and hcp superstructures usually consist of one particle type, or interlacing structures where two different building blocks arrange themselves each in a fcc structure and are combined together (such as the NaCl structure).

Depending on the size ratio of the particles ($\gamma_{AB} = R_B/R_A$), binary mixtures can even assemble into structures with packing densities larger than the fcc or hcp packing (∼0.74) where smaller particles fill the voids between larger particles.[15,16] Such structures are typically the most stable thermodynamically.[11,12,14] In fact, the size ratio and stoichiometry determine solely the lattice structure at equilibrium. For a low size ratio, $\gamma_{AB} < 0.4$, the typical stable structure is that of the AB$_n$ (NaCl for $n = 1$, AB$_2$ for $n = 2$, AB$_4$ for $n = 4$, *etc.*, depending on stoichiometry). For intermediate size ratios, $0.45 < \gamma_{AB} < 0.624$, structures of the type AB$_2$ are most stable. These include AlB$_2$ for $0.53 < \gamma_{AB} < 0.624$, HgBr$_2$ and AuTe$_2$ for $0.41 < \gamma_{AB} < 0.53$. NaZn$_{13}$ or orthorumbic-AB$_{13}$ are also predicted to be metastable in this range of size ratio.[17]

However, entropic considerations alone are insufficient to describe the diversity of structures observed by Shevchenko et al.[8] In particular, binary assemblies into low volume fraction superstructures cannot be explained by the hard spheres model.[18−20] These include, for example, the Cu_3Au type lattice for a size ratio of 0.58 or the $MgZn_2$ for a size ratio of 0.48. Thus, it remains a challenge to uncover the necessary or sufficient interactions leading to a diversity of binary superlattices of nanoparticles, regardless of whether these are at thermodynamic equilibrium or metastable structures.[21] What is the nature of interparticle interactions giving rise to a diversity of superstructures as well as quasicrystalline order beyond the simple hard spheres description? Shevchenko et al. pointed out that "it is specifically at the nanoscale that the van der Waals, electrostatic, steric repulsion, and the directional dipolar interactions can contribute to the interparticle potential with comparable weight. These, together with the effects of particle substrate interactions and space-filling (entropic) factors, combine to determine the binary superlattice structure."

An attempt to better understand the phase behavior of binary mixtures beyond the hard spheres model has recently been proposed by van Blaaderen an co-workers.[22] A combined experimental and theoretical study of ionic crystals of oppositely charged microparticles uncovered the role of long-range interactions.[23−26] Adding salts to the apolar colloidal suspensions offers control over the particle charge in addition to regulating the screening length. A pronounced phase change from NaCl to CsCl superstructure was observed as a function of the salt concentration, keeping the particle size fixed. Computer simulations based on the Yukawa model[27] gave a consistent picture with the experiments.

It is clear, however, that the description based on the Yukawa model cannot be valid for nanoparticles, where the dispersion interactions compete with the long-range electrostatic forces. This is a result of the smaller size of particles at the nanoscale that can account for small surface charges, thereby reducing the contribution of electrostatics in comparison with the large microparticles. Thus, it is expected that dispersion interaction will be of similar magnitude to the electrostatic forces. In this work, we explore the interplay between dispersion interactions and longer-range electrostatic forces by constructing a schematic phase diagram of binary mixtures of nanoparticles interacting via a combination of Hamaker and Yukawa potentials. We study the phase behavior as a function of the different model parameters including the size ratio of the nanoparticles, the charge ratio, and the ratio of electrostatic to dispersion interactions. In the Model Potential section we describe the model developed to study the interplay between dispersion interactions and longer-range electrostatic forces. The Results' section is dedicated to present the results and in the Discussion and Conclusions section we provide a discussion of the results and conclusions.

MODEL POTENTIAL

We assume that the total interaction potential can be described by a sum of pairwise interactions, where the pairwise potential includes a dispersion and screened Yukawa terms:

$$U_{ij}(r) = \nu U_{ij}^H(r) + (1 - \nu)U_{ij}^Y(r) \tag{1}$$

In the above, $U_{ij}(r)$ is the total two-body potential between particles $i \in A,B$ and $j \in A,B$, and ν is a parameter taken between 0 and 1. For $\nu = 0$ the model reduces to the Yukawa model while for $\nu = 1$ the model describes pure Hamaker-type interactions. Following the work of van Blaaderen and co-workers,[22] we describe the long-range electrostatic portion of the interactions between the nanoparticles by a Yukawa potential supplemented by a short-range repulsion term:

$$U_{ij}^Y(r) = U_{ij}^{HS}(r) + \alpha^Y Z_i Z_j \frac{\exp(-\kappa r)}{r} \tag{2}$$

where r is the distance between two particles, α^Y is a constant that determines the overall strength of the interactions, $Z_{i,j}$ is the charge number of particle $i,j \in A,B$, and κ is the reciprocal screening length. The first term in the above equation describes the hard core repulsion given by

$$U_{ij}^{HS}(r) = \begin{cases} 0 & r \geq \sigma_{ij} \\ U_{max}^{HS} & r < \sigma_{ij} \end{cases} \tag{3}$$

where σ_{ij} is the contact distance of two particles $\sigma_{ij} = R_i + R_j + \sigma_S$, $R_{i,j}$ is the radius of particle ij, $\sigma_S = {}^2/_3 R_B$ is used as a shell to circumvent the pathological behavior of the Hamaker potential (see eq 4 below), and $U_{max}^{HS} = 10000 K_B T$ such that further increasing the value of U_{max}^{HS} does not affect the results for the free energy (see below for further discussion).

The dispersive portion of the interaction potential is described by a Hamaker-type[28] combined with a sharp cutoff, given by

$$U_{ij}^H(r) = U_{ij}^{HS}(r) + \frac{-A_{ij}\Pi^2}{3}\left\{ R_j\left(\frac{r - R_i}{(r - R_i)^2 - R_j^2} - \frac{r + R_i}{(r+R_i)^2 - R_j^2}\right) \right.$$
$$+ \frac{1}{2}\ln\left(\frac{r^2 - (R_i + R_j)^2}{r^2 - (R_i - R_j)^2}\right)$$
$$\left. + \frac{R_j^3}{r}\left(\frac{1}{(r + R_i)^2 - R_j^2} - \frac{1}{(r - R_i)^2 - R_j^2}\right)\right\} \tag{4}$$

where A_{ij} is related to the Hamaker constant.

To reduce the number of parameters, we assume that both the Yukawa and the dispersion interactions share an identical contact energy of $-5K_B T$. This is obtained by adjusting the potential parameters according to

$$U_{AB}(\sigma_{AB}) = \nu U(\sigma_{AB})_{AB}^H + (1 - \nu)U(\sigma_{AB})_{AB}^Y$$
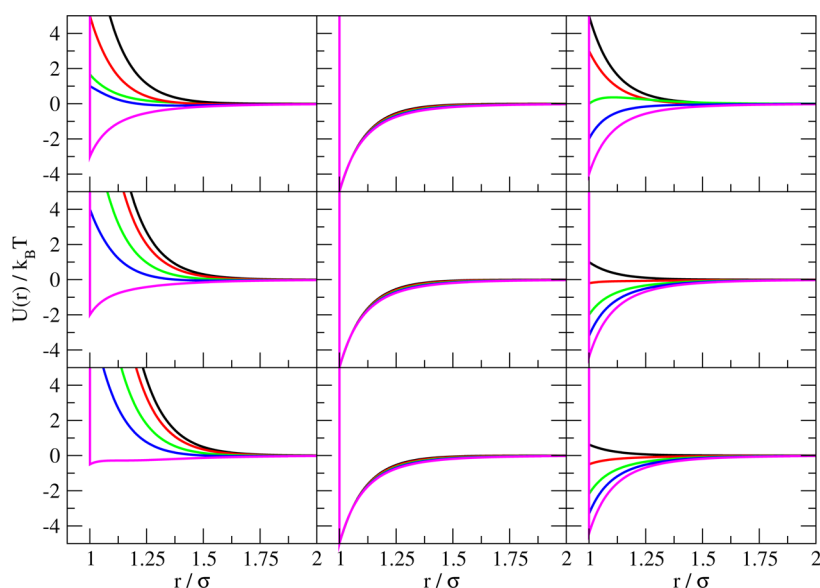$$= -5K_B T \tag{5}$$

for each value of ν.

Figure 1. Pair potential A−A (left panels), A−B (middle panels), and B−B (right panels) as a function of distance between particles, for three values of Q: $Q = 3$ (upper panels), $Q = 5$ (middle panels), and $Q = 8$ (lower panels). Black, red, green, blue, and magenta correspond to $\nu = 0$, $\nu = 0.2$, $\nu = 0.5$, $\nu = 0.7$, and $\nu = 0.9$, respectively. The results shown are for particles of similar size.

TABLE 1. Yukawa and Hamker Model Parameters[a]

γ_{AB}	$\alpha^Y Q$	A_{11}	A_{12}	A_{22}	κR_B
0.33	−6310	−12.067	−12.067	−12.067	1
0.50	−9843	−15.9	−15.9	−15.9	1.5
0.58	−10091	−16.1	−16.1	−16.1	1.74
0.68	−13649	−18.8	−18.8	−18.8	2.04
1.00	−39748	−31.2	−31.2	−31.2	3

[a] In all calculations $Z_B = 1$ and R_B is fixed. The units of A_{ij} is $k_B T$ and the units of α^Y is $k_B T \times R_B$.

In Figure 1 we plot the total pair potential between A−A, A−B, and B−B nanoparticles, for different values of ν and $Q = -Z_A/Z_B$. In all cases, the model parameters were adjusted so that the A−B contact interaction (the minimum of the pair-potential) was fixed at a value of $-5k_B T$. The parameters are summarized in Table 1. In all cases, regardless of the value of ν the A−B interactions are quite similar. However, as ν is increased the A−A and B−B repulsive interaction become attractive. The major effect of increasing the portion of dispersion forces is reflected in the A−A and B−B interactions, but not in the A−B interactions. This transition will play an important role in analyzing the superlattices of Shevchenko et al.[8]

RESULTS

We consider nine different superlattices, a subset of the structures reported by Shevchenko et al.[8] These include the NaCl, CsCl, Cu_3Au, AuCu, AlB_2, $MgZn_2$, Fe_4C, $CaCu_5$, and $NaZn_{13}$. A sketch of the crystal structures is shown in Figure 2, and a summary of the superstructures reported in ref 8 for different values of the size ratio is given in Table 2.
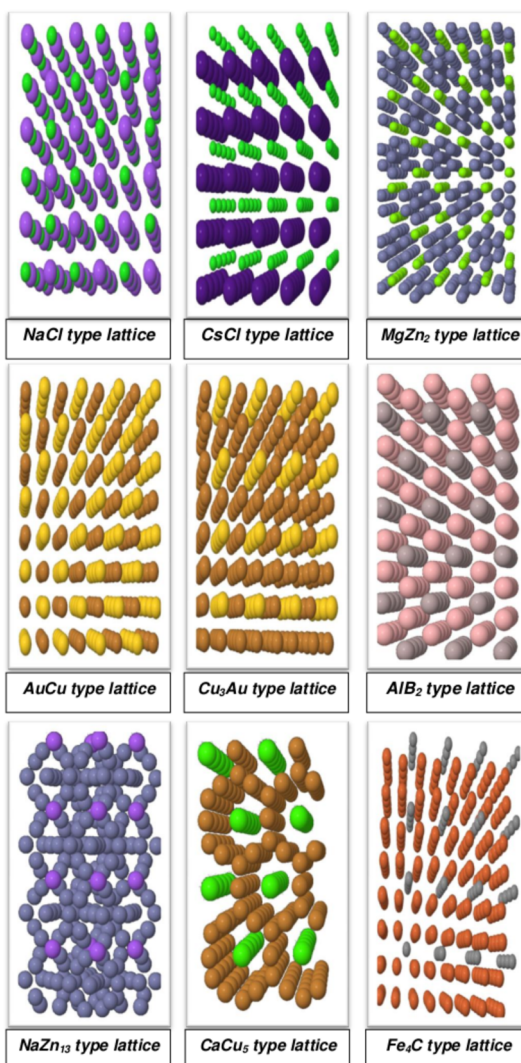

Figure 2. A sketch of the nine crystals structures studied.

The nine crystal structures provide a valuable set to assess the importance of competing interactions governing the formation of binary superlattices at the nanoscale. Not all structures can be derived from entropic consideration alone. For example, AuCu appears at $\gamma_{AB} \approx 0.66$ and CaCu$_5$ appears at $\gamma_{AB} \approx 0.69$. These structures are not metastable in the binary hard spheres model.[13] Moreover, some structures appear at size ratios outside the range found by the binary hard spheres model[14] or by the binary Yukawa model.[22] For example, the AlB$_2$ structure appears at $\gamma_{AB} = 0.45$ but is not a metastable structure of either of the aforementioned models.

For each system we have carried out a detailed analysis of the free energy based on the approach describe in the Methodology and Computational Details section. Calculations for the free energy were carried out only for systems that were stable during the constant pressure run. For the current model, the Fe$_4$C structure and the MgZn$_2$ structure observed experimentally[8] at $\gamma_{AB} = 0.48$ were computationally not stable for any set of model parameters studied.

TABLE 2. A Summary of the Structure Obtained in the Study of Shevchenko et al.[8a]

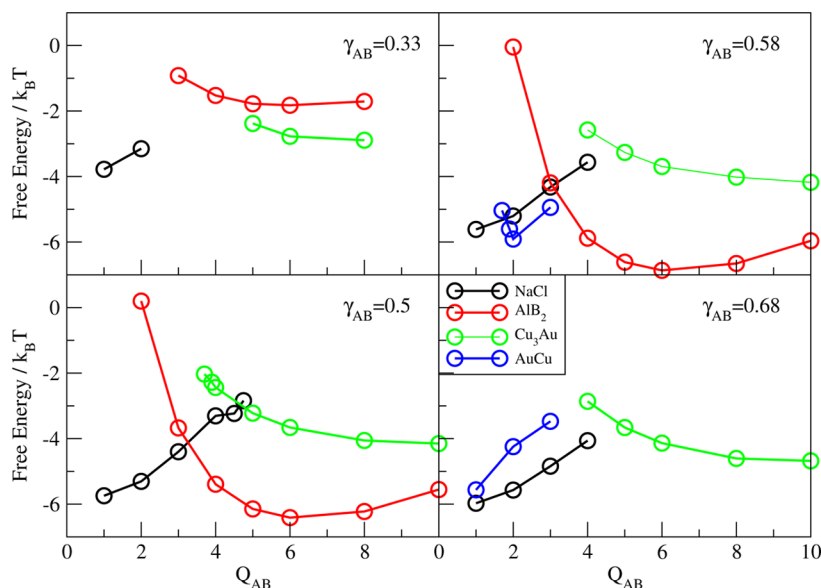| size ratio	structure
0.37 (5 nm/13.4 nm)	NaCl
0.45 (3 nm/6.7 nm)	AlB$_2$
0.48 (3 nm/6.2 nm)	MgZn$_2$, Fe$_4$C, cube-AB$_{13}$
0.52 (3 nm/5.8 nm)	CaB$_6$, MgNi$_2$
0.58 (4.2 nm/7.2 nm)	Cu$_3$Au, NaZn$_{13}$
0.66 (5 nm/7.6 nm)	AuCu
0.69 (5 nm/7.2 nm)	CaCu$_5$

[a] Note that the definition of γ_{AB} is based on the size ratio of the core of the nanocrystals similar to that in ref 8. More recently, Bodnarchuk et al.[31] also included corrections due to the ligand shell.

The simulation box consists of 216 nanoparticles for NaCl and AlB$_2$, 250 for CsCl, 256 nanoparticles were used to simulate the Cu$_3$Au and AuCu structures, 320 for Fe$_4$C, 192 for MgZn$_2$, 240 nanoparticles for CaCu$_5$, and 224 for NaZn$_{13}$. The inverse screening length in the Yukawa potential was taken to be $\kappa(R_B + \frac{1}{2}\sigma_S) = 4$. We studied the role of the aspect ratio $\gamma_{AB} = R_B/R_A$, the charge ratio $Q_{AB} = -Z_A/Z_B$ and the ratio of dispersion to electrostatic contribution to the interactions between the nanoparticle ν. All simulations were carried out at ambient conditions.

In Figure 3 we plot the free energy calculated for the pure electrostatic case, that is, $\nu = 0$ as a function of the charge ratio Q_{AB} for four different values of γ_{AB}. For each size ratio, only 3−4 structures were found to be metastable. For $\gamma_{AB} = \frac{1}{3}$ the NaCl structure is the only stable structure for $Q_{AB} \leq 2$ while for charge ratios larger than 4 we find that both Cu$_3$Au and AlB$_2$ are also metastable. In between these values of the charge ratios, the only metastable structure is the AlB$_2$. The results for small values of Q_{AB} are consistent with the hard spheres model, which also predicts the NaCl structure to be the stable one at $\gamma_{AB} = \frac{1}{3}$. The AlB$_2$ structure is likely to be stabilized by the electrostatic interactions at intermediate charge ratios and therefore does not appear at this size ratio for the hard spheres model.

As the size ratio is increased to $\frac{1}{2}$, the NaCl structure becomes metastable even at charge ratios of $Q_{AB} = 5$ and becomes unstable above this value. This is certainly different in comparison to the hard spheres model, where the most stable structure is predicted to be the AlB$_2$. The Cu$_3$Au structure is also metastable across a large range of Q_{AB} for $\gamma_{AB} = \frac{1}{2}$, even larger than the case of $\gamma_{AB} = \frac{1}{3}$.

This trend continues as the size ratio is further increased beyond $\frac{1}{2}$. At low values of Q_{AB}, the NaCl structure is

Figure 3. Free energy as a function of charge ratio Q_{AB} for four values of γ_{AB} and for $\nu = 0$, that is, the pure electrostatic case.
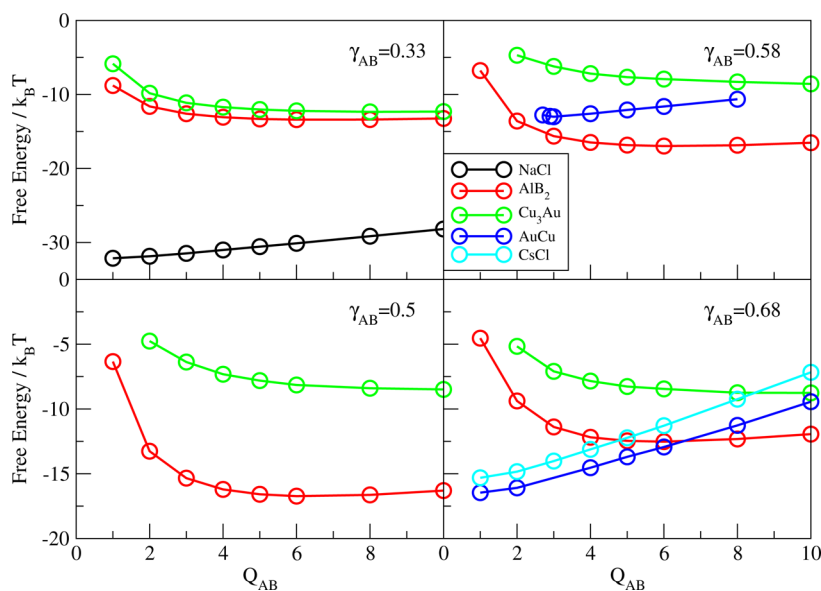
Figure 4. Free energy as a function of charge ratio Q_{AB} for four values of γ_{AB} and for $\nu = ^1/_2$.

still the only metastable structure. However, as $Q_{AB} \rightarrow 2$, the AuCu becomes metastable as well in the range of $2 \leq Q_{AB} \leq 3$. We note that Shevchenko *et al.* reported on the formation of Cu_3Au type structure for $\gamma_{AB} = 0.58$.[8] Our results for $\nu = 0$ suggest that the structure is metastable and could be stabilized by electrostatic interactions.

As the size ratio is further increased to $\gamma_{AB} = 0.68$, the picture changes qualitatively. The AlB_2 becomes unstable for any values of Q_{AB}. At lower value of Q_{AB} in the range $1 \leq Q_{AB} \leq 3$ both NaCl and AuCu structures are metastable. While NaCl has not been observed experimentally at this size ratio, AuCu has been reported by Shevchenko *et al.*[8] at $\gamma_{AB} = 0.66$.

In Figure 4 we plot the free energy calculated for the case $\nu = ^1/_2$ as a function of the charge ratio Q_{AB} for four different values of γ_{AB}. For each size ratio, only 2–4 structures were found metastable. Comparing the overall results to those shown in Figure 3 for the pure electrostatic case, we note that the free energy per nanoparticle is lower when dispersion interactions are introduced, despite the fact that the A—B contact interaction was fixed to $-5k_BT$. This can be traced to the change in the A—A and B—B interactions which at larger values of ν can even become attractive (see Figure 1).

At $\gamma_{AB} = ^1/_3$, we find three structures to be metastable, NaCl, AlB_2, and Cu_3Au across all values of Q_{AB}. This is in contrast to the pure electrostatic case, where the rocksalt is metastable at low values of Q_{AB} (and is unstable at high value of Q_{AB}) and the AlB_2 at high values of Q_{AB} (and is unstable at low values of Q_{AB}). At higher values of $\gamma_{AB} \geq 0.5$, the rocksalt structure becomes unstable for all values of Q_{AB}.

At $\gamma_{AB} = ^1/_2$ only two structures appear metastable— the AlB_2 structure and the Cu_3Au structure. This is consistent with the picture emerging for the hard

spheres model and the only major difference when dispersion interactions are introduced in addition to electrostatic forces is that the rocksalt structure becomes unstable at this size ratio. In general, we find that dispersion interactions favor the AlB_2 which is also the favorable structure of the hard spheres model. Comparing the results from the Cu_3Au structure, it is clear that it becomes relatively more stable at smaller values of Q_{AB} when dispersion interactions are switched on in comparison to the pure electrostatic case.

Returning to the results shown in Figure 4 for a size ratio $\gamma_{AB} = 0.58$, here, the AlB_2 is metastable across all values of Q_{AB}. AuCu becomes metastable at intermediate charge ratios, $2 \leq Q_{AB} \leq 8$, while Cu_3Au is metastable above $Q_{AB} \geq 2$. This is the structure that was observed experimentally for this size ratio.[8]

As we further increase the size ratio to $\gamma_{AB} = 0.68$ a new structure becomes metastable—the CsCl which is metastable for all charge ratios studied. This structure is further stabilized by dispersion interactions (see below). Furthermore, AuCu is also metastable for all charge ratios. This is consistent with the experimental results of Shevchenko *et al.* for size ratio of 0.66.[8] However, Shevchenko *et al.* also observed the $CaCu_5$ structure at size ratio of $\gamma_{AB} = 0.69$, while we find this structure to be unstable at all values of Q_{AB}. At larger charge ratios, above $Q_{AB} = 7$, the AlB_2 is still metastable, while for the pure electrostatic case, this structure was unstable, suggesting that the dispersion forces stabilize the AlB_2 structure.

The appearance of CsCl and AuCu at larger values of γ_{AB} is consistent with the space filling analysis of the hard spheres case.[31] The space filling factor of NaCl decreases below AlB_2 at $\gamma_{AB} > 0.45$ and space filling of CsCl and AuCu increases above that of NaCl at $\gamma_{AB} > 0.55$.
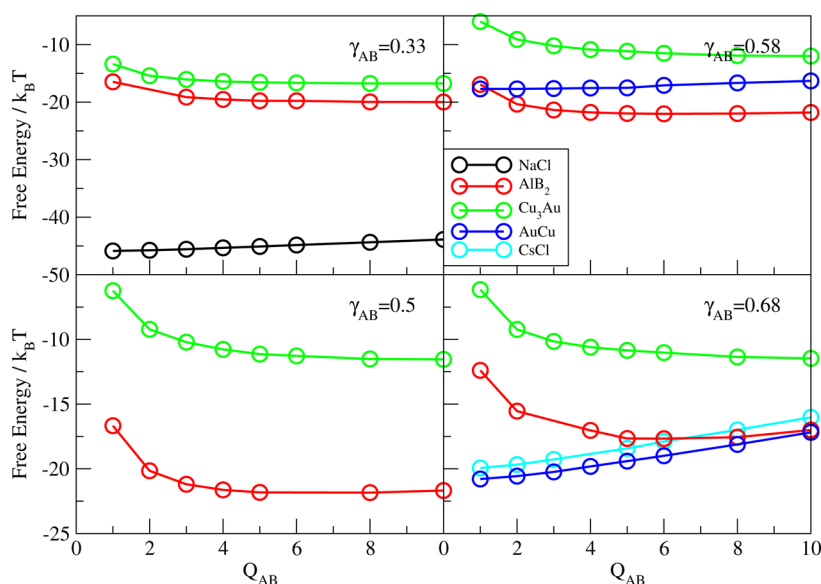
Figure 5. Free energy as a function of charge ratio Q_{AB} for four values of γ_{AB} and for $v = \frac{3}{4}$.

TABLE 3. Free Energy per Particle (in Units of $k_B T$) Results for Case of $v = 1$ for the Different Crystal Structures Studied

| size ratio	structure	free energy
0.33	NaCl	−51.8
	$NaZn_{13}$	−20.9
0.50	AlB_2	−19.8
0.58	$NaZn_{13}$	−29.4
	AlB_2	−17.8
	AuCu	−17.3
	$CaCu_5$	−3.8
0.68	CsCl	−18.0
	AuCu	−18.0
	AlB_2	−15.4
	$CaCu_5$	−6.8

In Figure 5 we plot the free energy calculated for the case $v = \frac{3}{4}$ as a function of the charge ratio Q_{AB} for the same four values of γ_{AB}. Similar to the case discussed above for $v = \frac{1}{2}$, the structures that were stabilized by dispersion interactions are stabilized even more when the portion of the dispersion is further increased. The major differences in comparison to the $v = \frac{1}{2}$ case are that the free energy of the NaCl structure is much lower for $\gamma_{AB} = \frac{1}{3}$ and the AuCu structure becomes metastable for all values of Q_{AB} for $\gamma_{AB} > \frac{1}{2}$. Qualitatively, for $\gamma_{AB} = 0.68$ the results are similar to the case of $v = \frac{1}{2}$.

In Table 3 we provide the results of the free energy calculations for the case of $v = 1$, where only dispersion interaction are included. For this case, at $\gamma_{AB} = \frac{1}{3}$, NaCl and $NaZn_{13}$ are the only metastable structures, similar to the hard spheres model. For $\gamma_{AB} = \frac{1}{2}$ the only metastable structure is AlB_2. Four structures appear to be metastable for a size ratio of $\gamma_{AB} = 0.58$: $NaZn_{13}$, AlB_2, AuCu, and $CaCu_5$. The latter appears to be stabilized only for the pure dispersive case. For the largest

size ratio of 0.68, Shevchenko et al.[8] reported the formation of the $CaCu_5$ structure. Once again, this structure is only stabilized when the dispersion interactions are dominant. We find three additional metastable structures at this size ratio: AuCu, CsCl, and AlB_2.

A summary of the results described in this section is given in Figure 6, where we plot a schematic phase diagram. The lines do not represent the exact phase boarder between different structures. We did perform other simulations within the range of size ratios in each case to confirm the general trends. We find that electrostatic interactions favor the AB structure (such as NaCl structure for small size ratios and AuCu for larger size ratios) at low charge ratios and AB_2 structure for intermediate to high charge ratios, irrespective of the size ratio. When dispersion interactions are added the behavior depends on the size ratio. For small size ratios, we find that dispersion interactions stabilize the NaCl for all charge ratios. At intermediate size ratios, typically the AlB_2 structure will be metastable across a wide range of size ratios. At high charge ratio, the addition of dispersion interactions stabilizes the AuCu structure. Two other points to be noted are the appearance of Cu_3Au only when electrostatic interactions are present and the appearance of $CaCu_5$ and $NaZn_{13}$ for the pure dispersive case.

With respect to the structures obtained experimentally,[8,32−35] one cannot overlook the importance of pure repulsion interactions. It seems that in most cases the denser structure is also the one observed experimentally.[8,32−35] This indicates that the regime at which these structures crystallize must be similar to that of the hard sphere model and can be explained by space filling analysis.[31] Yet there are deviations from the hard sphere case. Our model can capture both the hard sphere limit and also consistently account for
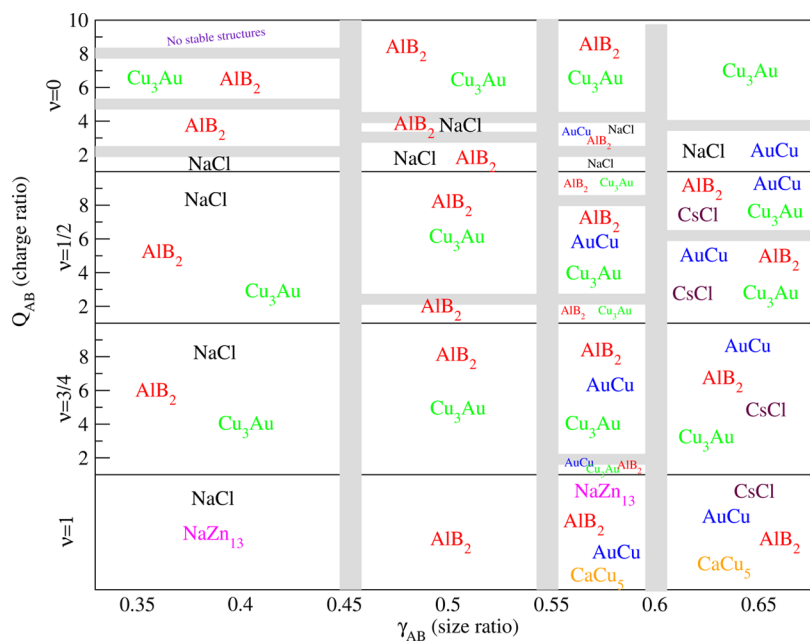
Figure 6. Schematic phase diagram showing the metastable structures for each value of ν, Q_{AB}, and γ_{AB}. The boundaries between phases are a sketch and were not determined precisely.

deviations from it. For example, the formation of binary structures at $\gamma_{AB} > 0.62$ cannot be explained from entropic considerations alone, since the hard sphere model will predict the formation of a phase-separated structure or a random close packing structure. In addition, low space filling structures, such as the Cu_3Au or the $CaCu_5$ are not predicted to occur in the hard spheres model.

DISCUSSION AND CONCLUSIONS

The goal of the present study was to understand the role of interactions between nanoparticles forming binary superlattices and the balance between electrostatic and dispersion interactions leading to the observed diversity of binary superlattices. To better understand the formation of the different superstructures and the interplay between dispersion and electrostatic interactions, we have carried out simulations of the stability of nine different binary superstructures. We find that neither electrostatic or entropic interactions alone explain the diversity of superstructures formed. Indeed, there is a strong correlation between structures with large space filling factor and those observed experimentally. However, in some cases we find deviations from this rule, which requires the addition of dispersion interactions to stabilize the observed structures at the correct size ratio. Moreover, we find a weak correlation between the metastable structures of the pure electrostatic case, some are of low space filling factors, and the structures observed experimentally. The following points support these conclusions:

(1) Our results suggest that NaCl is metastable for a broad range of size ratios only for the case of pure electrostatic interactions ($\nu = 0$) at relatively low charge ratios ($Q < 3$). The fact that NaCl appears at a size ratio $\gamma_{AB} > 0.37$ is not consistent with the experiments of Shevchenko *et al.*,[8] where NaCl appears only at $\gamma_{AB} = 0.37$. However, when dispersion interactions are introduced to our model, NaCl structure becomes metastable at size ratios $\gamma_{AB} < 0.45$, more consistent with the experiments.[8]

(2) A similar conclusion can be drawn for the case of the AuCu structure, which appears at a size ratio $\gamma_{AB} > 0.65$ as reported by Shevchenko *et al.*[8] Our results suggest that when dispersion interactions are included ($\nu > 0$), AuCu is metastable for low to intermediate values of Q_{AB}.

(3) Shevchenko *et al.*[8] reported that AlB_2 appears at a broad range of size ratios, most noticeably at a size ratio of $\gamma_{AB} = 0.45$ and $\gamma_{AB} = 0.68$. Once again, if only electrostatic interactions are considered, AlB_2 is not even metastable at size ratios $\gamma_{AB} > 0.6$. When dispersion interactions are included, AlB_2 becomes metastable at size ratios $\gamma_{AB} > 0.45$, consistent with the experiments. Furthermore, AlB_2 is the only metastable structure at $\gamma_{AB} < 0.45$ for intermediate charge ratios for the pure electrostatic case. However, this is not observed experimentally.

(4) Experimentally, at size ratios $\gamma_{AB} \geq 0.65$ either the $CaCu_5$ structure (with trioctylphosphine oxide (TOPO)) or AuCu structure (without TOPO) were observed. In this case, TOPO serves as a capping layer reducing the net charge on the particles. This would translate to a change in Q_{AB}, but more importantly to a change in ν diminishing the electrostatic contribution. Furthermore, at size ratio of 0.58, electro-mobility measurements indicate that $CaCu_5$ structure is metastable with vanishing charges.[33] Our results suggest that these structures are metastable for the pure dispersion case

($\nu = 1$) for size ratios $\gamma_{AB} \geq 0.55$ and when electrostatic interactions were included ($0 < \nu < \frac{1}{2}$), AuCu structure is metastable only when $\gamma_{AB} \geq 0.55$, while $CaCu_5$ becomes unstable. These results suggest that (a) electrostatic interactions alone are not sufficient to explain the experimental results of AuCu and $CaCu_5$, and (b) when $CaCu_5$ is observed, electrostatic interactions are negligible, consistent with the effect of capping with TOPO.

(5) The special case of size ratio $\gamma_{AB} = 0.58$ demonstrates the delicate interplay between electrostatic and dispersion interactions. Experimentally, at this size ratio the metastable structures found were Cu_3Au, $NaZn_{13}$, $CaCu_5$ and AlB_2.[8,32,33] While the results of Shevchenko et al. for the former two were explained by electrostatic interactions,[8] the latter two structures were shown to form with vanishing charges.[32,33] Our results are consistent with both reports, showing that the Cu_3Au structure is stabilized only when electrostatic interactions are included while $NaZn_{13}$ and $CaCu_5$ structures are stabilized by dispersion interactions alone.

In summary, considering the nine different superstructures and comparing the results obtained in the experiments, we believe that both electrostatic and dispersion interactions need to be considered in the assembly of binary mixtures of nanoparticles. We find that consistency with experiments is obtained when dispersion interactions supplement the electrostatics, and often are even more important. The most diverse set of structures consistent with experiments appears when $\nu \geq \frac{3}{4}$ and when $Q \leq 5$. Indeed, at this regime, the phase behavior is quite different from that of colloidal particles at the micrometer scale, and the diversity of superstructures is much richer. Perhaps, tuning the screening length or turning to the regime $0 < Q_{AB} < 1$ may lead to a better agreement between the model and experiments. This and other topics are open for future study.

METHODOLOGY AND COMPUTATIONAL DETAILS

Thermodynamic Integration. To obtain the free energy of the different crystal structures we follow a thermodynamic integration scheme starting from the Einstein crystal.[29] The approach is slightly different from the original work of Frenkel and Ladd[30] in the specific integration method and in the way we account for pressure:

(1) We start from a Monte Carlo (MC) simulation at constant pressure (NPT ensemble) for a given set of model parameters and a given crystal structure to obtain the average volume at ambient conditions ($P = 1$ atm, $T = 300$ K). We used 500 000 MC steps to equilibrate the system starting from the ideal volume and an additional 500 000 MC steps were used for data acquisitions. During this run, structures that were not stable for a given set of model parameters were not included in the next thermodynamic integration step.

(2) A thermodynamic integration scheme for a canonical ensemble (NVT) was used to obtain the free energy of the different crystal structures, where the volume was taken as the average volume in the NPT run. The thermodynamic integration was carried with respect to the Einstein crystal, $F - F_{Ein} = \int_0^1 d\lambda \langle U_\lambda(\mathbf{r}, \lambda) \rangle_\lambda$,[29] where the integration variable λ was defined according to

$$U_\lambda(r) = (1 - \lambda)U(r) + \lambda U_{Ein}(\mathbf{r})$$

$$U(r) = \sum_{i > j}^{N} \nu U_{ij}^{H}(r_{ij}) + (1 - \nu)U_{ij}^{Y}(r_{ij})$$

$$U_{Ein}(\mathbf{r}) = \alpha \sum_{j}^{N} (r_j - r_j^0)^2 \tag{6}$$

In eq 6, $\mathbf{r}$ is a shorthand notation for the position vector of all nanoparticles, $\mathbf{r}_j$ is the position vector of particle j, r_{ij} is the distance between nanoparticle i and j, $\mathbf{r}_j^0$ is the position vector of nanoparticle j in a specific crystal structure, N is the total number of nanoparticles in the system, and α is a spring constant determined according to ref 29. We used a simple Gauss-Laguerre integration scheme with 20 sampling points. The value of U_{max}^{HS} was chosen such that $\lambda_{min} U_{max}^{HS}$ was sufficiently large to prevent particles from interpenetrating during the thermodynamic integration. The cutoff distances were taken to be $2.5\sigma_{ij}$. For all cases the energy at the cutoff distances was $\leq 10^{-6} k_B T$. For each value of λ, 200 000 MC steps were carried both for equilibration and data acquisitions, separately.

The above procedure was repeated for each crystal structure and for each set of model parameters, that is, for different values of κ, Q, ν, and size ratio of nanoparticles. In Table 4 we summarize the results of the above procedure for the single component hard spheres model and compare our approach with the original study of Frenkel and Ladd (FL).[30] The overall agreement is excellent with differences smaller than 0.5% for the larger system sizes.

Conflict of Interest: The authors declare no competing financial interest.

TABLE 4. The Excess Free Energy in Units of $k_B T$ per Nanoparticle for the Hard Spheres Model for fcc and hcp Crystal Structures. The Reduced Density is $\rho^* = 0.736$

lattice	f_{ex} (FL)	f_{ex}	N
fcc	5.891	5.806	96
hcp	5.899	5.802	96
fcc	5.903	5.879	192
hcp	5.905	5.878	192
fcc	5.916	5.879	216
hcp	5.917	5.882	216

REFERENCES AND NOTES

1. Shelby, R. A.; Smith, D. R.; Schultz, S. Experimental Verification of a Negative Index of Refraction. *Science* **2001**, *292*, 77–79.
2. Shalaev, V. M. Optical Negative-Index Metamaterials. *Nat. Photon.* **2007**, *1*, 41–48.
3. Pendry, J. Negative Refraction. *Contemp. Phys.* **2004**, *45*, 191–202.
4. Shevchenko, E. V.; Talapin, D. V.; Rogach, A. L.; Kornowski, A.; Haase, M.; Weller, H. Colloidal Synthesis and Self-Assembly of CoPt₃ Nanocrystals. *J. Am. Chem. Soc.* **2002**, *124*, 11480–11485.
5. Redl, F. X.; Cho, K.-S.; Murray, C. B.; O'Brien, S. Three-Dimensional Binary Superlattices of Magnetic Nanocrystals

and Semiconductor Quantum Dots. *Nature* **2003**, *423*, 968–971.

6. Talapin, D. V.; Koeppe, R.; Götzinger, S.; Kornowski, A.; Lupton, J. M.; Rogach, A. L.; Benson, O.; Feldmann, J.; Weller, H. Highly Emissive Colloidal CdSe/CdS Heterostructures of Mixed Dimensionality. *Nano Lett.* **2003**, *3*, 1677–1681.

7. Shevchenko, E. V.; Talapin, D. V.; O'Brien, S.; Murray, C. B. Polymorphism in AB13 Nanoparticle Superlattices an Example of Semiconductor Metal Metamaterials. *J. Am. Chem. Soc.* **2005**, *127*, 8741–8747.

8. Shevchenko, E. V.; Talapin, D. V.; Kotov, N. A.; O'Brien, S.; Murray, C. B. Structural Diversity in Binary Nanoparticle Superlattices. *Nature* **2006**, *439*, 55–59.

9. Urban, J. J.; Talapin, D. V.; Shevchenko, E. V.; Kagan, C. R.; Murray, C. B. Synergism in Binary Nanocrystal Superlattices Leads to Enhanced p-Type Conductivity in Self-Assembled PbTe/Ag$_2$Te Thin Films. *Nat. Mater.* **2007**, *6*, 115–121.

10. Talapin, D. V.; Shevchenko, E. V.; Bodnarchuk, M. I.; Ye, X.; Chen, J.; Murray, C. B. Quasicrystalline Order in Self-Assembled Binary Nanoparticle Superlattices. *Nature* **2009**, *461*, 964–967.

11. Murray, M. J.; Sanders, J. V. Close-Packed Structures of Spheres of Two Different Sizes I. Observations on Natural Opal. *Philos. Mag. A* **1980**, *42*, 705–720.

12. Murray, M. J.; Sanders, J. V. Close-Packed Structures of Spheres of Two Different Sizes II. The Packing Densities of Likely Arrangements. *Philos. Mag. A* **1980**, *42*, 721–740.

13. Eldridge, M. D.; Madden, P. A.; Frenkel, D. Entropy-Driven Formation of a Superlattice in a Hard-Sphere Binary Mixture. *Nature* **1993**, *365*, 35–37.

14. Hopkins, A. B.; Stillinger, F. H.; Torquato, S. Densest Binary Sphere Packings. *Phys. Rev. E* **2012**, *85*, 125501.

15. Hudson, T. S.; Harrowell, P. Dense Packings of Hard Spheres of Different Sizes Based on Filling Interstices in Uniform Three-Dimensional Tilings. *J. Phys. Chem. B* **2008**, *112*, 8139–8143.

16. KummerFeld, J. K.; Hudson, T. S.; Harrowell, P. The Densest Packing of AB Binary Hard-Sphere Homogeneous Compounds Across All Size Ratios. *J. Phys. Chem. B* **2008**, *112*, 10773–10776.

17. Hudson, T. S. Dense Sphere Packing in the NaZn13 Structure Type. *J. Phys. Chem. C* **2010**, *114*, 14013–14017.

18. Min, Y.; Akbulut, M.; Kristiansen, K.; Golan, Y.; Israelachvili, J. The Role of Interparticle and External Forces in Nanoparticle Assembly. *Nat. Mater.* **2008**, *7*, 527–538.

19. Rechtsman, M.; Stillinger, F.; Torquato, S. Designed Interaction Potentials *via* Inverse Methods for Self-Assembly. *Phys. Rev. E* **2006**, *73*, 011406.

20. Rechtsman, M. C.; Stillinger, F. H.; Torquato, S. Synthetic Diamond and Wurtzite Structures Self-Assemble with Isotropic Pair Interactions. *Phys. Rev. E* **2007**, *75*, 031403.

21. Sztrum, C.; RABani, E. Out-of-Equilibrium Self-Assembly of Binary Mixtures of Nanoparticles. *Adv. Mater.* **2006**, *18*, 565–571.

22. Leunissen, M. E.; Christova, C. G.; Hynninen, A.-P.; Royall, C. P.; Campbell, A. I.; Imhof, A.; Dijkstra, M.; van Roij, R.; van Blaaderen, A. Ionic Colloidal Crystals of Oppositely Charged Particles. *Nature* **2005**, *437*, 235–240.

23. Bier, M.; van Roij, R.; Dijkstra, M. Phase Diagrams of Binary Mixtures of Oppositely Charged Colloids. *J. Chem. Phys.* **2010**, *133*, 124501.

24. Hynninen, A.; Christova, C.; van Roij, R.; van Blaaderen, A.; Dijkstra, M. Prediction and Observation of Crystal Structures of Oppositely Charged Colloids. *Phys. Rev. Lett.* **2006**, *96*, 138308.

25. Hynninen, A.-P.; Panagiotopoulos, A. Z. Phase Diagrams of Charged Colloids from Thermodynamic Integration. *J. Phys.: Condens. Matter* **2009**, *21*, 465104.

26. Vernizzi, G.; Zhang, D.; de la Cruz, M. O. Structural Phase Transitions and Mechanical Properties of Binary Ionic Colloidal Crystals at Interfaces. *Soft Matter* **2011**, *7*, 6285–6293.

27. Yukawa, H. On the Interaction of Elementary Particles. *Proc. Phys. Math. Soc. Jpn.* **1935**, *17*, 48–57.

28. Hamaker, H. C. The London van der Waals Attraction between Spherical Particles. *Physica* **1937**, *4*, 1058–1072.

29. Frenkel, D.; Smith, B. *Understanding Molecular Simulation*; Academic Press: San Diego, 2002.

30. Frenkel, D.; Ladd, A. J. C. New Monte Carlo Method to Compute the Free Energy of Arbitrary Solids. Application to the FCC and HCP Phases of Hard Spheres. *J. Chem. Phys.* **1984**, *81*, 3188–3193.

31. Bondnarchuk, M. I.; Kovalenko, M. V.; Heiss, W.; Talapin, D. V. Energetic and Entropic Contributions to Self-Assembly of Binary Nanocrystal Superlattices, Temptor as the Structure Directing Factor. *J. Am. Chem. Soc.* **2010**, *132*, 11967–11977.

32. Chen, J.; Xingchen, C. Systematic Electron Crystallographic Studies of Self Assembled Binary Nanocrystal Superlattices. *ACS Nano* **2010**, *4*, 2374–2381.

33. Chen, Z.; Moore, J.; Radtke, G.; Sirringhaus, H.; O'Brien, S. Binary Nanoparticle Superlattices in the Semiconductor Semiconductor System CdTe and CdSe. *J. Am. Chem. Soc.* **2007**, *129*, 15702–15709.

34. Bartlett, P.; Ottewill, R. H.; Pusey, P. N. Superlattice Formation in Binary Mixtures of Hard-Sphere Colloids. *Phys. Rev. Lett.* **1992**, *68*, 3801–3804.

35. Shevchenko, E. V.; Talapin, D. V.; Murray, C. B.; O'Brien, S. Structural Characterization of Self-Assembled Multifunctional Binary Nanoparticle Superlattices. *J. Am. Chem. Soc.* **2006**, *128*, 3620–3637.